Determination of retardation parameters of multiple-order wave plate using a phase-sensitive heterodyne ellipsometer

Cheng-Hung Hsieh,[1] Chien-Chung Tsai,[1] Hsiang-Chun Wei,[1] Li-Ping Yu,[2] Jheng-Syong Wu,[3] and Chien Chou[1,2,3,*]

[1]Institute of Biophotonics, National Yang Ming University, Taipei, Taiwan 112
[2]Institute of Radiological Sciences, National Yang Ming University, Taipei, Taiwan 112
[3]Institute of Optical Sciences, National Central University, Jhongli, Taiwan 320

*Corresponding author: cchou@ym.edu.tw

Received 21 March 2007; revised 5 June 2007; accepted 5 June 2007;
posted 5 June 2007 (Doc. ID 81166); published 9 August 2007

To characterize the linear birefringence of a multiple-order wave plate (MWP), an oblique incidence is one of the methods available. Multiple reflections in the MWP are produced, and oscillations in the phase retardation measurement versus the oblique incident angle are then measured. Therefore, an antireflection coated MWP is required to avoid oscillation of the phase retardation measurement. In this study, we set up a phase-sensitive heterodyne ellipsometer to measure the phase retardations of an uncoated MWP versus the oblique incident angle, which was scanned in the x–z plane and y–z plane independently. Thus, the effect on multiple reflections by the MWP is reduced by means of subtracting the two measured phase retardations from each other. As a result, a highly sensitive and accurate measurement of retardation parameters (RPs), which includes the refractive indices of the extraordinary ray n_e and ordinary ray n_o, is obtained by this method. On measurement, a sensitivity (n_e, n_o) of 10^{-6} was achieved by this experiment setup. At the same time, the spatial shifting of the P and S waves emerging from the MWP introduced a deviation between experimental results and the theoretical calculation.

OCIS codes: 120.3180, 040.2840, 120.5050, 120.5410.

1. Introduction

A multiple-order wave plate (MWP) can adjust the polarization state of light waves, and this is achieved by changing its thickness or using a different wavelength of light wave. Furthermore, the polarization state can also be adjusted by tilting the wave plate such that the laser beam is obliquely incident onto the wave plate [1,2]. To do this, the retardation parameters (RPs) of an MWP, including the refractive indices of extraordinary ray (E-ray) n_e and ordinary ray (O-ray) n_o and the order number of the interference m are required. Preuss and Gole [3] derived an explicit Jones transformation matrix for a tilted wave plate with its optical axis on the surface plane. However, spatial beam splitting with respect to the E-ray and O-ray was ignored. Zhu [4] developed a modified Jones transformation matrix where the spatial beam splitting effect is considered because an optical path difference is introduced between the E-ray and O-ray in the MWP. However, the modified explicit Jones transformation matrix does not consider the effects of multiple reflections [5] and the spatial shifting of the emerging beams simultaneously. Pietraszkiewicz *et al.* [5] proved numerically that there are multiple reflections produced at near normal incidence in a quartz wave plate. Recently, Jeng and Lo [6] successfully demonstrated a heterodyne polariscope that was able to measure

0003-6935/07/235944-07$15.00/0

RPs sequentially by the use of an antireflection MWP where the oblique incident angle was limited to a range of less than 5°. Their method requires two tested samples of which the difference in thickness is less than 30 μm to assure that both samples have an equal order number of the interference for calibration purposes. In this study, we set up a phase-sensitive optical heterodyne ellipsometer to measure the phase retardation of the P and S waves for measurement of the RPs [7,8]. The multiple reflections and the spatial shifting effect of the emerging beams are considered such that high sensitivity for the RPs measurement at a large oblique incident angle becomes applicable. Experimentally, a sensitivity (n_e, n_o) for detection in the order of 10^{-6} was achieved due to a phase stability of 0.3°/h during measurement.

2. Principle

In Fig. 1, a polarized common-path optical heterodyne ellipsometer is set up [8] in which two acousto-optic modulators (AOMs) are driven at frequencies of ω_1 and ω_2 in the reference and signal channels, respectively. A linearly polarized laser beam is incident into the Mach–Zehnder interferometer such that the P_1 and S_1 waves are in the reference channel whereas the P_2 and S_2 waves are in the signal channel. Both P waves ($P_1 + P_2$) are mixed together to produce a P–polarized heterodyne signal with a beat frequency of $\Delta\omega$ at the photodetector D_p. Simultaneously, an S-polarized heterodyne signal is generated by S_1 and S_2 waves at the photodetector D_s. They are expressed by

$$I_p(\Delta\omega t) = |E_{p_1} + E_{p_2}|^2 = I_{p_1} + I_{p_2} + 2\sqrt{I_{p_1} I_{p_2}}\cos(\Delta\omega t + \delta_p), \quad (1)$$

$$I_s(\Delta\omega t) = |E_{s_1} + E_{s_2}|^2 = I_{s_1} + I_{s_2} + 2\sqrt{I_{s_1} I_{s_2}}\cos(\Delta\omega t + \delta_s), \quad (2)$$

where $\delta_p = \delta_{p_2} - \delta_{p_1}$, $\delta_s = \delta_{s_2} - \delta_{s_1}$ are the phase difference between the P_1 and P_2 waves and between the S_1 and S_2 waves, respectively. Meanwhile, (I_{p_1}, δ_{p_1}), (I_{p_2}, δ_{p_2}), (I_{s_1}, δ_{s_1}), and (I_{s_2}, δ_{s_2}) are the intensities and phases of P_1, P_2, S_1, and S_2 waves, accordingly. To analyze the state of polarization quantitatively, a parameter X is defined [7] by

$$X = \frac{E_s}{E_p}\exp[i(\delta_s - \delta_p)] = |X|\exp[i\delta], \quad (3)$$

where E_p and E_s are the amplitudes of the P and S waves, respectively, and δ_p and δ_s are their phases, accordingly. Therefore, the elliptical polarization at the output of the system $X^{(o)}$ is determined by the elliptical polarization at the input of the system $X^{(i)}$ where the bilinear transformation can be described as

$$X^{(o)} = \frac{T_{22} + X^{(i)}T_{21}}{T_{12} + X^{(i)}T_{11}}, \quad (4)$$

and the coefficients T_{11}, T_{12}, T_{21}, and T_{22} are the elements of corresponding Jones matrix [9],

$$T_\varepsilon = \begin{bmatrix} T_{11} & T_{12} \\ T_{21} & T_{22} \end{bmatrix} = \begin{bmatrix} \cos\frac{\gamma}{2} + i\cos 2\varepsilon \sin\frac{\gamma}{2}\cos 2\left(\theta + \frac{\pi}{2}\right) & \sin\frac{\gamma}{2}\sin 2\varepsilon + i\cos 2\varepsilon \sin\frac{\gamma}{2}\sin 2\left(\theta + \frac{\pi}{2}\right) \\ -\sin\frac{\gamma}{2}\sin 2\varepsilon + i\cos 2\varepsilon \sin\frac{\gamma}{2}\sin 2\left(\theta + \frac{\pi}{2}\right) & \cos\frac{\gamma}{2} - i\cos 2\varepsilon \sin\frac{\gamma}{2}\cos 2\left(\theta + \frac{\pi}{2}\right) \end{bmatrix}. \quad (5)$$

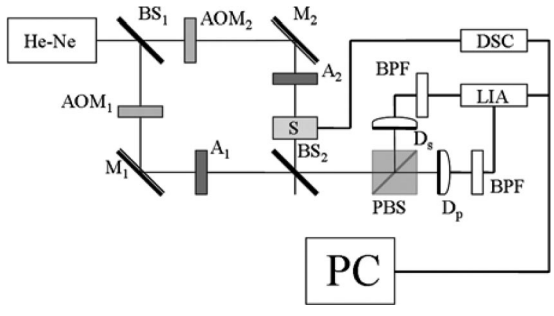

Fig. 1. Experimental setup: **BS$_1$**, **BS$_2$**: beam splitters, **AOM$_1$**, **AOM$_2$**: acousto-optic modulators, **M$_1$**, **M$_2$**: mirrors, **A$_1$**, **A$_2$**: analyzers, **S**: test sample on rotation stage, **PBS**: polarization beam splitter, **D$_p$**, **D$_s$**: photo detectors, **BPF**: band-pass filter, **LIA**: lock-in amplifier, **DSC**: digital stepping controller, **PC**: personal computer.

In the experiment (Fig. 1), the initial state of polarization at $X^{(i)} = 1$ (i.e., $|X^{(i)}| = 1$ and $\delta^{(i)} = 0°$) is adjusted [9] while no tested sample is inserted and the azimuth angles of the polarizers A_1 and A_2 in the reference and signal channels are adjusted at 45° to the x-axis. Then, Eq. (4) is simplified to

$$X^{(o)} = \frac{T_{22} + T_{21}}{T_{12} + T_{11}}. \quad (6)$$

The phase difference between the P and S waves of the emerging beam from the tested MWP becomes

$$\delta_\varepsilon{}^{(o)} = \tan^{-1}\left(\left\{2\sin\frac{\gamma}{2}\cos 2\varepsilon\left[\sin\frac{\gamma}{2}\sin 2\varepsilon\sin 2\left(\theta+\frac{\pi}{2}\right) - \cos\frac{\gamma}{2}\cos 2\left(\theta+\frac{\pi}{2}\right)\right]\right\}\Big/\left[\cos^2\frac{\gamma}{2} - \sin^2\frac{\gamma}{2}\sin^2 2\varepsilon - \frac{1}{2}\sin^2\frac{\gamma}{2}\cos^2 2\varepsilon\cos 4\left(\theta+\frac{\pi}{2}\right)\right]\right), \quad (7)$$

where θ is the orientation of slow eigenelliptical polarization from the x-axis and $\varepsilon = \tan^{-1}(b/a)$ is the ellipticity angle of the eigenpolarizations of the MWP, where a and b are the lengths of the major and minor axes of the polarization ellipse [7]. Furthermore, $\gamma = 2\pi(n_s - n_f)d/\lambda$ is the phase retardation between the fast and slow eigenelliptical polarizations and n_f and n_s are the refractive indices with respect to two eigenelliptical polarizations, accordingly [5,7,8]. The thickness d and wavelength λ are available in this setup. A linearly polarized laser beam is normally incident onto an MWP of which the optical axis is on its surface [x–y plane in Fig. 2(a)]. Then, the MWP is rotated along the z-axis of the propagation direction of the laser beam for phase retardation $\delta_\varepsilon{}^{(o)}(\theta)$ measurement using a lock-in amplifier. The condition $\varepsilon = 0$ is satisfied because the MWP is considered to be a linear birefringent material and multiple reflections by the MWP are not considered at this moment. Then, Eq. (7) can be described by

$$\delta_\varepsilon{}^{(o)} = \tan^{-1}\left(\left\{2\sin\frac{\gamma}{2}\left[-\cos\frac{\gamma}{2}\cos 2\left(\theta+\frac{\pi}{2}\right)\right]\right\}\Big/\left[\cos^2\frac{\gamma}{2} - \frac{1}{2}\sin^2\frac{\gamma}{2}\cos 4\left(\theta+\frac{\pi}{2}\right)\right]\right). \quad (8)$$

The laser beam is obliquely incident onto the surface of MWP in which the initial conditions of n_e for the polarization of the E-ray along the x-axis and n_o for the polarization of the O-ray along the y-axis as shown in Fig. 2(b). The y-axis is parallel to the surface of the MWP, and ϕ_o and $\tilde{\phi}_e$ are the refractive angles with respect to the O-ray and $\tilde{E}$-ray of the MWP. When the incident angle ϕ_{ty} is scanned in the x–z plane, $\tilde{n}_e$ is expressed by [10] $\tilde{n}_e = n_e n_o/\sqrt{{n_o}^2\cos^2\tilde{\phi}_e + {n_e}^2\sin^2\tilde{\phi}_e}$. Thus, the phase difference between the $\tilde{E}$-ray and O-ray emerging from the MWP can be expressed by [11]:

$$\begin{aligned}\delta_{ty} &= \delta_s - \delta_p \\ &= \frac{2\pi}{\lambda}(n_o\overline{AC}) - \frac{2\pi}{\lambda}(\tilde{n}_e\overline{AD} + \overline{DE}) \\ &= \frac{2\pi}{\lambda}d(n_o\cos\phi_o - \tilde{n}_e\cos\tilde{\phi}_e) \\ &= \frac{2\pi}{\lambda}d\left(\sqrt{{n_o}^2 - \sin^2\phi_{ty}} - \sqrt{{n_e}^2 - \frac{{n_e}^2}{{n_o}^2}\sin^2\phi_{ty}}\right), \end{aligned} \quad (9)$$

where δ_{ty} is a function of ϕ_{ty}, n_e, and n_o. The spatial splitting of the $\tilde{E}$-ray and O-ray, which introduces an

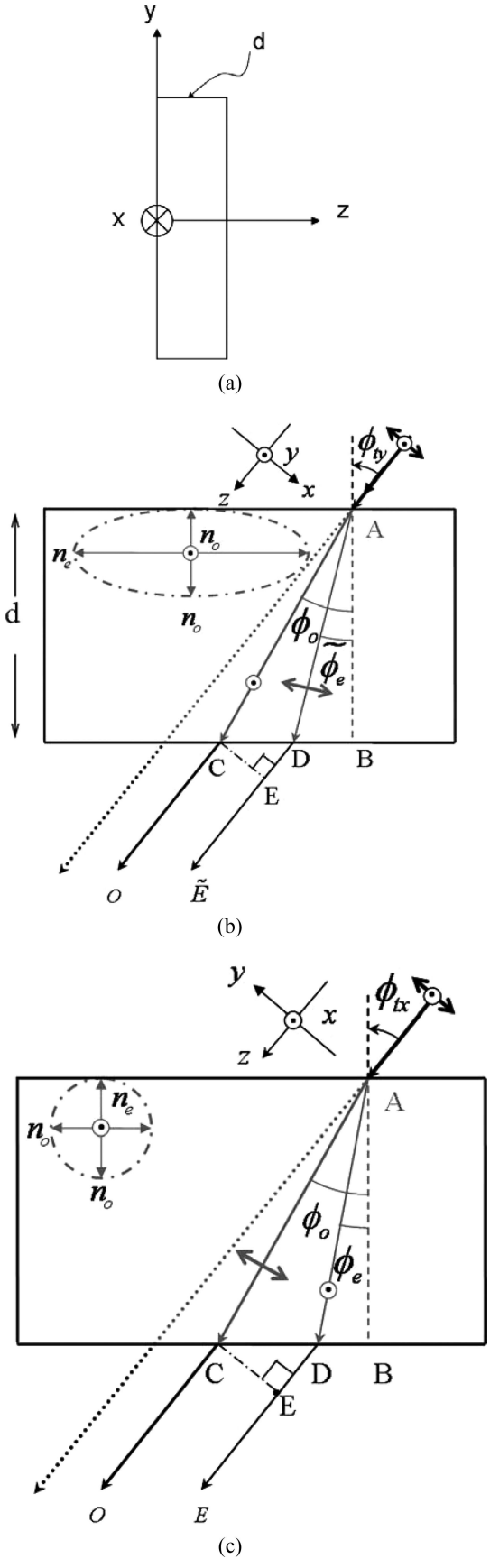

Fig. 2. (a) Schematic diagram of normal incidence. (b) Schematic diagram of the oblique incident angle in the x–z plane. (c) Schematic diagram of the oblique incident angle in the y–z plane.

optical path difference of the MWP, is included. Therefore, the difference between δ_{ty} and δ_0, which is the phase retardation at normal incident, becomes

$$\delta_{ty} - \delta_0 = \frac{2\pi}{\lambda} d\left[\left(\sqrt{{n_o}^2 - \sin^2\phi_{ty}} - \sqrt{{n_e}^2 - \frac{{n_e}^2}{{n_o}^2}\sin^2\phi_{ty}}\right) - (n_o - n_e)\right], \tag{10}$$

where $\delta_0 = 2\pi(n_o - n_e)d/\lambda$; $\delta_{ty} = \delta_s - \delta_p$ is the phase retardation of the S and P waves of the MWP at an oblique incident angle of ϕ_{ty} in the x–z plane. Similarly, the oblique incident angle ϕ_{tx} is scanned in the y–z plane of the MWP, where it is under the initial conditions of n_e for polarization along the x-axis and n_o for polarization along the y-axis, while ϕ_o and ϕ_e are the refractive angles of O-ray and E-ray, respectively [see Fig. 2(c)]. Then, the phase difference δ_{tx} from δ_0 becomes

$$\delta_{tx} - \delta_0 = \frac{2\pi}{\lambda} d\left[\left(\sqrt{{n_o}^2 - \sin^2\phi_{tx}} - \sqrt{{n_e}^2 - \sin^2\phi_{tx}}\right) - (n_o - n_e)\right], \tag{11}$$

where $\delta_{tx} = \delta_s - \delta_p$ is the phase retardation of the S and P waves at incident angle ϕ_{tx} in the y–z plane.

For a linearly birefringent medium ($\varepsilon = 0$), γ becomes equal to Γ where $0° \le \Gamma \le 360°$. However, the true phase retardation of the MWP is expressed by

$$\frac{2\pi}{\lambda} d(n_e - n_o) = 2m\pi + \Gamma. \tag{12}$$

However, the effect of multiple reflections needs to be considered at an oblique incidence. According to Hecht [11], the multiple-reflection effect of an uncoated MWP at a small tilted incident angle generates an extra phase retardation Δ_{tx} in the x–z plane or Δ_{ty} in the y–z plane. This is expressed by

$$\Delta = \tan^{-1}\left[\frac{{r_s}^2 \sin\Gamma_s}{{r_s}^2\cos\Gamma_s - 1}\right] - \tan^{-1}\left[\frac{{r_p}^2\sin\Gamma_p}{{r_p}^2\cos\Gamma_p - 1}\right], \tag{13}$$

where Δ is the extra phase retardation between the E-ray and O-ray. In the case of an MWP that is tilted along the y-axis (in the x–z plane), then $\Delta = \Delta_{ty}$ in Eq. (13), where $r_s = r_{sy} = (n_o - n_{air})/(n_o + n_{air})$ and $r_p = r_{py} = (\tilde{n}_e - n_{air})/(\tilde{n}_e + n_{air})$ are expressed. Meanwhile, $\Gamma_s = \Gamma_{sy} = 2\pi/\lambda(d(2n_o\cos\phi_o))$ and $\Gamma_p = \Gamma_{py} = 2\pi/\lambda(d(2\tilde{n}_e\cos\tilde{\phi}_e))$ are defined as well. Similarly, Δ becomes Δ_{tx} when ϕ_{tx} of the MWP is scanned along the x-axis (in the y–z plane). Then, $r_s = r_{sx} = (n_o - n_{air})/(n_o + n_{air})$ and $r_p = r_{px} = (n_e - n_{air})/(n_e + n_{air})$ are expressed. $\Gamma_s = \Gamma_{sx} = 2\pi/\lambda(d(2n_o\cos\phi_o))$ and $\Gamma_p = \Gamma_{px} = 2\pi/\lambda(d(2n_e\cos\phi_e))$ are defined accordingly. Figures 3(a) and 3(b) are the computer simulations of

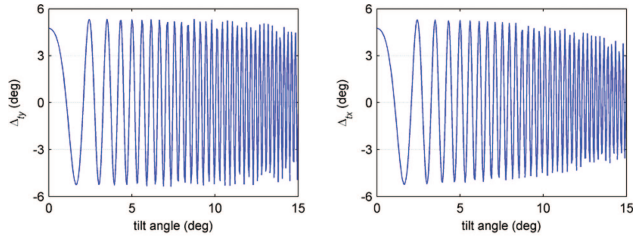

(a) (b)

Fig. 3. (Color online) Computer simulations of phase retardations due to multiple reflections of an uncoated QWP tilted in the x–z plane (a) Δ_{ty} and (b) Δ_{tx} tilted in the y–z plane where $n_e = 1.5518$, $n_o = 1.5428$, and $d = 0.506$ mm with tilted angle ϕ_{ty} at $\lambda = 632.8$ nm.

Δ_{ty} and Δ_{tx} versus the tilted angles ϕ_{ty} and ϕ_{tx}, respectively. To reduce the multiple-reflection effect, δ_{ty} is subtracted from δ_{tx} at $\phi_{ty} = \phi_{tx} = \phi_t$ and the common multiple reflection effect is therefore effectively cancelled. Thus,

$$(\delta_{ty} - \delta_{tx})/(2m\pi + \Gamma) = \left(\sqrt{{n_e}^2 - \sin^2\phi_t} - \sqrt{{n_e}^2 - {n_e}^2\sin^2\phi_t/{n_o}^2}\right)\Big/(n_e - n_o). \tag{14}$$

The (n_e, n_o, m) are then obtained from Eq. (14), using the least square error fitting between the experimental data and Eq. (14) where the thickness of the MWP and the wavelength λ are given.

3. Experimental Setup and Results

The experimental setup is shown in Fig. 1. Two multiple-order quarter wave plates (QWPs) with or without antireflection coating were tested in this experiment where $\varepsilon \cong 0°$ (linear birefringence) and the optical axis on the surface of the QWP are satisfied. The phase retardation of $\delta^{(o)}(\theta)$ versus the rotation angle θ along the z-axis at normal incidence is measured where each rotation step is 1° using a digital

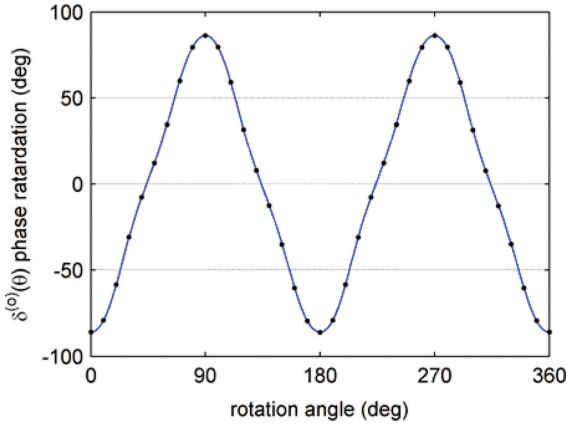

Fig. 4. (Color online) Experimental results (dots) for phase retardation $\delta^{(o)}(\theta)$ versus rotation angle θ of an uncoated QWP at normal incidence. The theoretical calculation (solid curve) is $\delta^{(o)}(\theta - \theta_{min})$ after an angle being shifted.

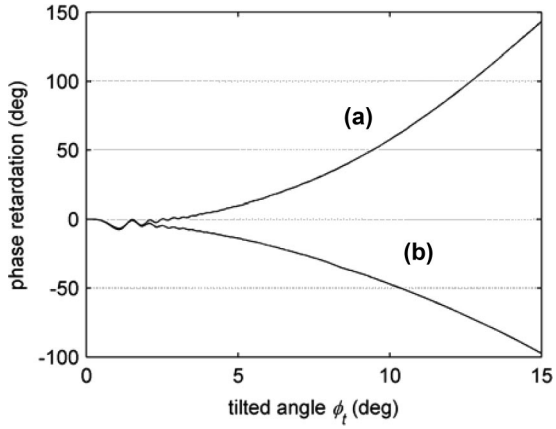

Fig. 5. (a) $\delta_{ty}(\phi_{ty}) - \delta_0$ and (b) $\delta_{tx}(\phi_{tx}) - \delta_0$ versus ϕ_{ty} and ϕ_{tx} of an uncoated QWP where $\phi_{ty} = \phi_{tx} = \phi_t$ is arranged.

stepping controller (DSC). During the measurements, the optical axis is aligned with the x-axis by rotating the test QWP, and then Eq. (8) is satisfied. An uncoated QWP was tested first in which multiple reflections are considered. The phase retardation of the P and S waves versus rotation angle θ at normal incident was measured. Thus, $\gamma = \delta_o = 86.28°$, $\theta_{shift} = -89°$, and $\varepsilon = 1.22°$ were obtained by curve fitting between the measured data and Eq. (8) of $\delta^{(o)}(\theta - \theta_{shift})$. The θ_{shift} is induced by the optical components in the interferometer [9]. The correlation between the experimental results (dots) and theoretical calculation (solid curve) is 0.999990 as shown in Fig. 4 in which the residual phase retardation from optical components in the interferometer is offset numerically [9]. Next, the uncoated QWP was rotated along the y-axis in the range of $0° \le \phi_{ty} \le 15°$ for phase retardation $\delta_{ty}(\phi_{ty})$ measurement. Then, $\delta_{ty}(\phi_{ty}) - \delta_o$ was calculated as shown in curve (a) in Fig. 5. Similarly, $\delta_{tx}(\phi_{tx}) - \delta_o$ was measured as well when the oblique incident angle ϕ_{tx} is along the x-axis in the range of $0° \le \phi_{tx} \le 15°$, which is shown in Fig. 5(b). The oscillations in Fig. 5 are clearly seen at a small rotated angle. This is in contrast to the result where

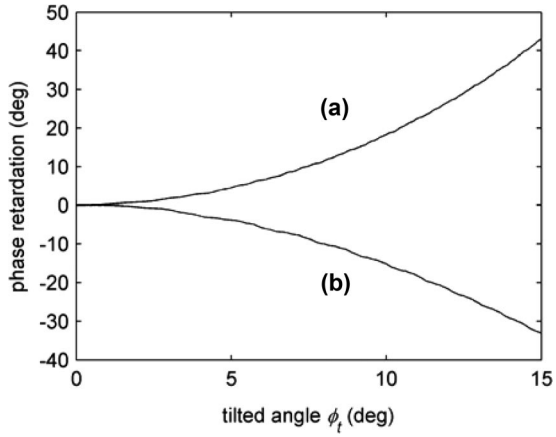

Fig. 6. Phase retardations of (a) $\delta_{ty}(\phi_{ty}) - \delta_0$ and (b) $\delta_{tx}(\phi_{tx}) - \delta_0$ of an antireflection QWP under the condition of $\phi_{ty} = \phi_{tx} = \phi_t$.

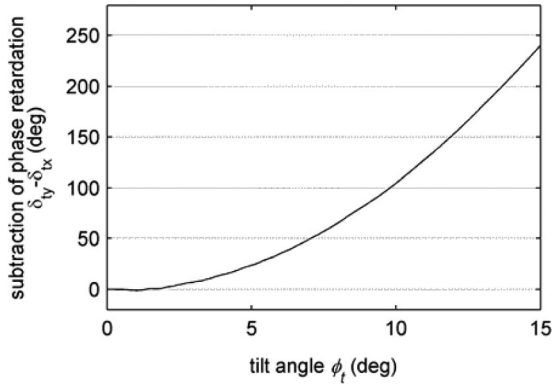

Fig. 7. Oscillations are eliminated in $\delta_{ty} - \delta_{tx}$ of an uncoated QWP at a condition of $\phi_{ty} = \phi_{tx} = \phi_t$.

there are no oscillations in phase retardation when testing an antireflection QWP as shown in Figs. 6(a) and 6(b) by scanning ϕ_{ty} and ϕ_{tx} along the y-axis and x-axis, respectively. As a result, the presence of multiple reflections that cause oscillation in oblique incident phase retardation of an uncoated QWP is experimentally verified. Thus, $\delta_{ty} - \delta_0$ and $\delta_{tx} - \delta_0$ can be subtracted from each other under the arrangement of $\phi_{ty} = \phi_{tx} = \phi_t$ such that the effect of multiple reflections is effectively eliminated. Figure 7 shows the result of $\delta_{ty} - \delta_{tx}$ for the tested uncoated QWP in this experiment. It is apparent that there is no oscillation of $\delta_{ty} - \delta_{tx}$ in the range $0° \le \phi_t \le 15°$. Interestingly, we found that on testing an antireflected QWP without multiple reflections, the measured $\delta_{ty}(\phi_{ty}) - \delta_0$ [Fig. 8(a)] and $\delta_{tx}(\phi_{tx}) - \delta_0$ [Fig. 8(b)] do deviate from Eqs. (10) and (11), respectively, at large oblique incident angles. These are caused by a spatial shifting of the P and S waves when they emerge from the tested QWP as shown in Fig. 9. This is introduced by the beam splitting of the E-ray and O-ray at the front surface of the QWP at oblique incidence in Figs. 2(b) and 2(c). The spatial shifting effect of the emerg-

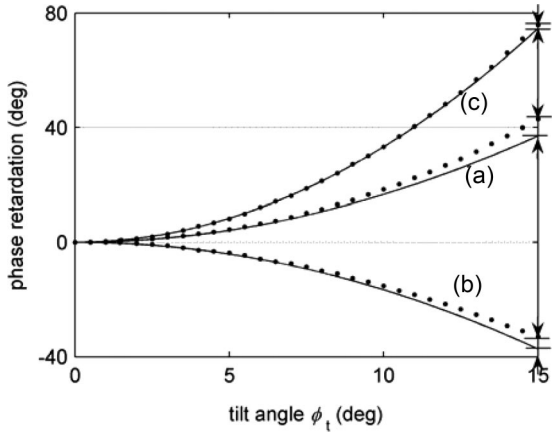

Fig. 8. Measured (a) $\delta_{ty}(\phi_{ty}) - \delta_0$ versus ϕ_{ty} and (b) $\delta_{tx}(\phi_{tx}) - \delta_0$ versus ϕ_{tx} of an antireflection QWP where $\phi_{ty} = \phi_{tx} = \phi_t$. Dots are the measured data while the solid curve shows the calculated data based on $n_e = 1.5518$, $n_o = 1.5428$, and $d = 0.506$ mm, at $\lambda = 632.8$ nm. (c) Result of $\delta_{ty} - \delta_{tx}$.

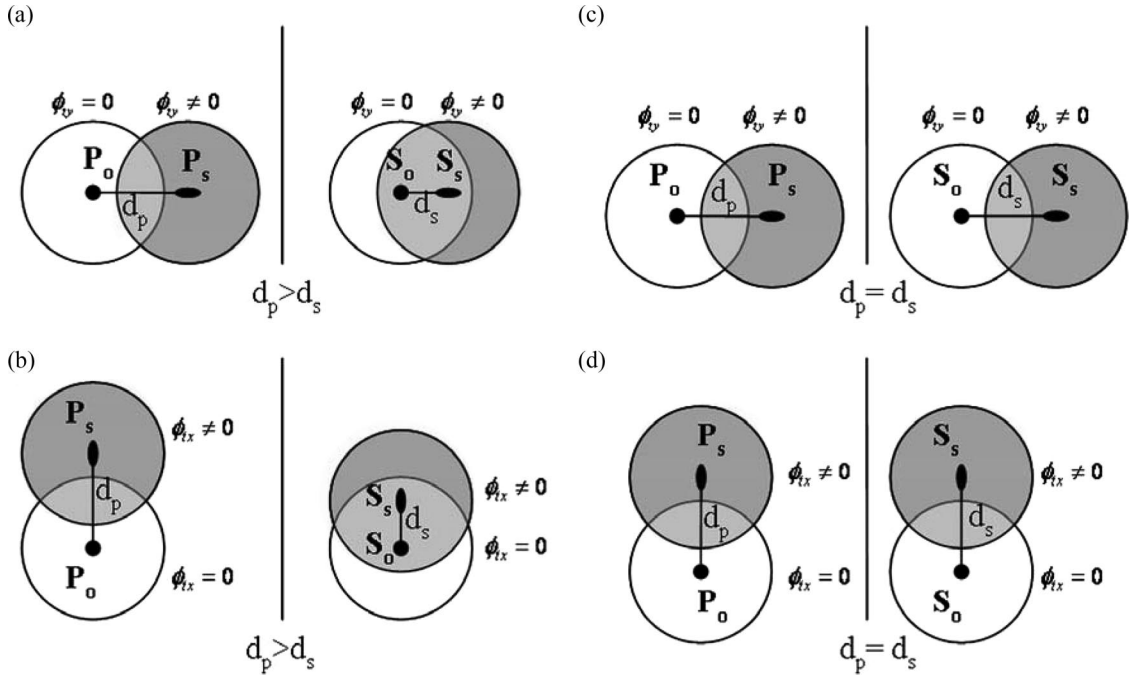

Fig. 9. Spatial shifting of emerging laser beams from an anisotropic wave plate ($d_p > d_s$) and an isotropic glass plate ($d_p = d_s$) of (a) and (c), respectively, where the angle is tilted in the x–z plane and of (b) and (d), where the angle is tilted in the y–z plane. P_0 and S_0 are the position of P and S waves at $\phi_{ty} = 0$ and $\phi_{tx} = 0$, respectively.

ing beams can be explained in Fig. 9, in which different amounts of displacement of the P and S waves occur as they emerge from QWP at the large angles of ϕ_{ty} and ϕ_{tx}. Obviously, an improvement in the reduction of the deviation occurs when we subtract curve (a) and curve (b) as shown in Fig. 8(c). Similarly, a common error is induced when the spatial shifting effect in $\delta_{ty} - \delta_0$ and $\delta_{tx} - \delta_0$ is canceled by subtraction. From Fig. 8(c), the value $n_e - n_o = 0.00908$ was calculated based on the experimentally calculated data for the order number $m = 7$ and the given thickness $d = 0.506$ mm of the antireflected coated QWP, and then $n_o = 1.54188$ and $n_e = 1.55096$ were obtained by the best curve-fitting of Fig. 8(c) with Eq. (14). When these results are compared with the reference data for the quartz wave plate [12] ($n_o = 1.5427$, $n_e = 1.5518$), the percentage error is 0.05% for the refractive indices of O-ray and E-ray, respectively. During the measurement, the phase stability of this experiment was 0.3°/h. This implies that the detection sensitivity for refractive index measurement is $\delta n = (\lambda/2\pi)(\delta\phi/d) \simeq 10^{-6}$.

4. Discussion and Conclusion

In this study, a phase-sensitive optical heterodyne ellipsometer is set up to measure the RPs of an uncoated MWP precisely. An oblique incidence of the laser beam is scanned in this experiment and tilted phase retardation measurement carried out. Thus, the multiple reflections by an uncoated multiple-order QWP at a small oblique incident angle can be eliminated efficiently. At the same time, the spatial shifting effect at large oblique incident angles can be effectively reduced by subtracting the two tilted phase retardations along the x-axis and y-axis. As a result, an extension on the dynamic range of the scanned oblique incident angle is possible, which improves the accuracy of RPs measurement. In summary, a method able to precisely measure (n_o, n_e, m) of an MWP by use of pure phase-sensitive detection, rather than amplitude-sensitive detection, involving an optical heterodyne ellipsometer, is experimentally demonstrated. This is possible because of the common path configuration of this optical heterodyne interferometer, which results in the common phase noise and environmental disturbance being removed effectively in phase retardation measurement. Thus, the stability of the phase retardation detection in this interferometer is better than that found using amplitude measurement and provides high sensitivity and accuracy when carrying out RPs measurements [13]. The multiple-reflection effect and the spatial shifting effect are reduced in this experimental setup. This method is then able to extend tilted phase retardation into a larger oblique incident and this assures high accuracy for the RPs measurements with both antireflected coated and uncoated MWPs.

This research was supported by the National Science Council of Taiwan through grant NSC-94-2215-E-010-001.

References

1. J. Mentel, E. Schmidt, and T. Mavrudis, "Birefringent filter with arbitrary orientation of the optic axis: an analysis of improved accuracy," Appl. Opt. **31,** 5022–5029 (1992).
2. X. Wang and J. Yao, "Transmitted and tuning characteristics of birefringent filters," Appl. Opt. **31,** 4505–4508 (1992).
3. D. R. Preuss and J. L. Gole, "Three-stage birefringent filter

tuning smoothly over the visible region: theoretical treatment and experimental design," Appl. Opt. **19,** 702–710 (1980).
4. X. Zhu, "Explicit Jones transformation matrix for a tilted birefringent plate with its optic axis parallel to the plate surface," Appl. Opt. **33,** 3502–3506 (1994).
5. K. Pietraszkiewicz, W. A. Wozniak, and P. Kurzynowski, "Effect of multiple reflections in retardation plates with elliptical birefringence," J. Opt. Soc. Am. A **12,** 420–424 (1995).
6. Y. T. Jeng and Y. L. Lo, "Heterodyne polariscope for sequential measurements of the complete optical parameters of a multiple-order wave plate," Appl. Opt. **45,** 1134–1141 (2006).
7. R. M. A. Azzam and N. M. Bashara, *Ellipsometry and Polarized Light* (North–Holland, 1979), p. 99.
8. C. Chou, Y. C. Huang, and M. Chang, "Effect of elliptical birefringence on the measurement of the phase retardation of a quartz wave plate by an optical heterodyne polarimeter," J. Opt. Soc. Am. A **14,** 1367–1372 (1997).
9. C. C. Tsai, C. Chou, C.–Y. Han, C.–H. Hsieh, K.–Y. Liao, and Y.–F. Chao, "Determination of optical parameters of a twisted-nematic liquid crystal by phase-sensitive optical heterodyne interferometric ellipsometry," Appl. Opt. **44,** 7509–7514 (2005).
10. E. D. Palik, *Handbook of Optical Constants of Solids III* (Academic, 1998), p. 729.
11. E. Hecht, *Optics* (Addison–Wesley, 1998), pp. 409–412.
12. *Optics Guide* (CASIX, Inc., 1995), p. 1 [no = 1.5427, no = 1.5518 (633 nm)].
13. P. D. Hale and G. W. Day, "Stability of birefringent linear retarders (wave plates)," Appl. Opt. **27,** 5146–5153 (1988).